

Gravitational Wavetrains in the Quasi-Equilibrium Approximation: A Model Problem in Scalar Gravitation

Hwei-Jang Yo^{1,2}, Thomas W. Baumgarte¹, and Stuart L. Shapiro^{1,3}

¹*Department of Physics, University of Illinois at Urbana-Champaign, Urbana, IL 61801*

²*Institute of Astronomy and Astrophysics, Academia Sinica, Taipei 115, Taiwan, ROC*

³*Department of Astronomy & NCSA, University of Illinois at Urbana-Champaign, Urbana, IL 61801*

A quasi-equilibrium (QE) computational scheme was recently developed in general relativity to calculate the complete gravitational wavetrain emitted during the inspiral phase of compact binaries. The QE method exploits the fact that the gravitational radiation inspiral timescale is much longer than the orbital period everywhere outside the ISCO. Here we demonstrate the validity and advantages of the QE scheme by solving a model problem in relativistic scalar gravitation theory. By adopting scalar gravitation, we are able to numerically track without approximation the damping of a simple, quasi-periodic radiating system (an oscillating spherical matter shell) to final equilibrium, and then use the exact numerical results to calibrate the QE approximation method. In particular, we calculate the emitted gravitational wavetrain three different ways: by integrating the exact coupled dynamical field and matter equations, by using the scalar-wave monopole approximation formula (corresponding to the quadrupole formula in general relativity), and by adopting the QE scheme. We find that the monopole formula works well for weak field cases, but fails when the fields become even moderately strong. By contrast, the QE scheme remains quite reliable for moderately strong fields, and begins to breakdown only for ultra-strong fields. The QE scheme thus provides a promising technique to construct the complete wavetrain from binary inspiral outside the ISCO, where the gravitational fields are strong, but where the computational resources required to follow the system for more than a few orbits by direct numerical integration of the exact equations are prohibitive.

I. INTRODUCTION

The construction of several new gravitational wave detectors, including the Laser Interferometer Gravitational Wave Observatory (LIGO), TAMA, VIRGO and GEO, may soon make gravitational wave astronomy a reality. The inspiral and coalescence of compact binaries, consisting of neutron stars or black holes, are among the most promising sources for detection by these observatories. It is expected that neutron star/neutron star binaries will spend approximately 16,000 cycles in the LIGO/VIRGO frequency band, neutron star/black hole binaries about 3,500, and black hole/black hole binaries about 600 [1]. To increase the likelihood of detection, and to extract information from the signal, the binary inspiral has to be modeled theoretically and waveform templates have to be constructed.

The evolution of compact binaries proceeds in different stages. By far the longest is the initial quasi-equilibrium inspiral stage, during which the compact objects move in nearly circular orbits, while the separation between them slowly decreases as energy is carried away by gravitational radiation. The quasi-circular orbits become unstable at the innermost stable circular orbit (ISCO), where the inspiral enters a plunge and merger phase. The merger and coalescence happens on a dynamical timescale, and produces either a black hole or, for binary neutron stars, possibly a larger neutron star, which may collapse to a black hole at a later time. The final stage of the evolution is the ringdown phase, during which the

merged object settles down to equilibrium.

Two distinct approaches have commonly been employed to analyze the adiabatic inspiral phase. Much progress has been made in post-Newtonian studies of compact binaries (see e.g. [2] and references therein). Most of these approaches, however, approximate the compact objects as point sources, which neglects important finite-size effects which may be particularly important for neutron star binaries. Also, PN expansions may not converge sufficiently rapidly in the strong-field region near the ISCO. Alternatively, compact binaries can be modeled numerically. Computational constraints currently limit dynamical evolution calculations to at most a few orbits, so that there is no hope to simulate a complete inspiral. It is possible, however, to numerically model binaries in the adiabatic inspiral phase in a quasi-equilibrium (QE) approximation.

The QE approximation is based on the assumption that the gravitational radiation reaction time scale is much longer than the orbital timescale, so that the binary can be approximated to be in quasi-equilibrium (and quasi-circular orbit) on an orbital timescale. A similar approximation is routinely being used in stellar evolution calculations. There, the evolutionary timescale is much longer than the hydrodynamical timescale, so that the star can safely be assumed to be in quasi-equilibrium on a dynamical timescale. Quasi-equilibrium models of compact binaries have been constructed both for neutron stars (see, e.g., [3] for corotating and [4] for irrotational binary neutron stars) and for black holes [5].

Even though individual QE models only represent “snap-shots” of binaries at a certain separation, it is possible to construct the complete adiabatic inspiral together with the emitted gravitational wave signal using the following scheme [6]. For each separation, a QE model can be inserted as a matter source into Einstein’s equations (this is the “hydro-without-hydro” approach demonstrated in [7]). Numerically integrating Einstein’s equations for this given matter source will then yield the gravitational wave signal and luminosity of the binary at that separation. Interpolation between a discrete sample of separations then yields the gravitational wave luminosity as a continuous function of separation. Combining this with the binary’s binding energy as a function of separation, one can construct the inspiral rate at all separations, and hence the separation as a function of time. Given a suitable parameterization, the entire continuous inspiral wavetrain can then be constructed. The viability of this approach has recently been demonstrated in [8] where a prototype calculation was presented for corotating binary neutron stars obeying a polytropic equation of state. Note that unlike post-Newtonian approaches, the QE scheme uses the fully nonlinear Einstein equations. The QE approach is also computationally very efficient, since it is possible to produce a very large number of cycles from a small number of QE configurations, each of which needs to be followed for only a couple of orbital periods.

In this paper, we evaluate the QE approach for a model problem in relativistic scalar gravitation, and show that it produces excellent agreement with an exact numerical solution. While scalar gravity (see, e.g., problem 7.1 in Misner, Thorne and Wheeler [9]) is not the correct theory of gravitation, it is conceptionally much simpler than general relativity (GR), and shares many of its characteristic features. This makes scalar gravity a very attractive framework for calibrating the QE approximation scheme, since, unlike in GR, we can directly compare its results with the readily producible exact solution.

In scalar gravity, the gravitational field is described by one scalar function. Also, scalar gravity generates gravitational radiation even in spherical symmetry, so that the generation and emission of gravitational waves can be studied with a spherically symmetric numerical code, involving only one spatial coordinate. This enables us to track the effect of radiation reaction exactly over many dynamical timescales. Moreover, outgoing wave boundary conditions can be imposed correctly at arbitrarily close separations from the sources in spherical symmetry, which eliminates the need for large computational grids. The theory also admits a local law of energy conservation, while GR only obeys global energy conservation. In numerical work, such a conservation law provides a strong check on the accuracy of integration. For all of these reasons, scalar gravitation has been employed successfully to develop many tools of numerical relativity (see, e.g., Shapiro and Teukolsky [10], hereafter ST, and also [11]) and we extend that tradition here.

In this paper we study, in the framework of scalar gravitation, the damped oscillations of a spherical matter shell, which we adopt as a simple spherically symmetric analogue to binary inspiral in GR. A relativistic binary emits gravitational waves, which slowly extracts energy from the binary orbit, so that the inspiral proceeds along a sequence of nearly periodic circular orbits of decreasing separation. Similarly, an oscillating matter shell emits gravitational waves, which slowly extracts energy from the oscillation, so that the damping proceeds along a sequence of nearly periodic oscillations of decreasing amplitude. Similar to relativistic binaries, where we consider the quasi-circular orbits at a certain separation of the adiabatic inspiral to be in QE, we may also consider the matter shell’s quasi-periodic oscillations of a certain amplitude to be in QE. One difference between the two processes is that the binary inspiral continues until coalescence and merger, while the damping of the matter shell’s oscillations will continuously slow down until a true equilibrium state has been reached.

We adopt three distinct approaches to computing the damped oscillation of the matter shell. We first compute the exact solution, by numerically integrating the exact equations. In our second approach, we adopt a QE approximation by neglecting gravitational waves, and computing QE models of the periodic, undamped oscillations of matter shells for various oscillation amplitudes. These QE models are then inserted as matter sources into the dynamical equations for the gravitational field. Integrating the field equations for these QE matter sources yields the gravitational wave form and luminosity for each oscillation amplitude. Combining the wave luminosity with the QE oscillation energy as a function of amplitude yields the amplitude decay rate together with the continuous gravitational wavetrain. This is the analogue to the QE approach to binary inspiral as outlined above. In a third approach, we use a monopole formula to compute the gravitational waveforms and wave luminosity for QE models and hence to determine the inspiral rate. This is the equivalent to using the quadrupole formula in GR to compute the inspiral rate and waveforms for binary models.

We compare these three different approaches for three different initial configurations, representing weak, moderately strong and ultra-strong field cases. We find that for the weak field configuration, all three approaches agree very well. For the moderately strong field configuration, the QE approach still agrees very well with the exact solution, while the agreement with the monopole result is much worse. Only for ultra-strong fields, for which the assumptions of QE break down, do we find a disagreement between the QE approach and the exact solution. However, even in this case, the break-down is gradual and not abrupt. This is a very encouraging result, and suggests that the QE approach is a very reliable and efficient framework for computing adiabatic binary inspiral up to the ISCO.

The paper is organized as follows. We summarize the

basic equations of scalar gravity in Sec. II, and outline the QE scheme in the Sec. III. In Sec. IV we present our numerical results, and compare our three approaches for the three different situations. We summarize and discuss the implications of our findings in Sec. V. We also include three Appendices. Appendix A contains a short proof that a minimum in the quasi-equilibrium energy corresponds to a static equilibrium shell solution. Appendix B presents some details of the QE scheme for constructing a continuous wavetrain. Appendix C describes our numerical implementation of the field equation. Throughout the paper we adopt gravitational units with $G = c = 1$.

II. THE BASIC EQUATIONS

A. Dynamical equations

We follow exercise (7.1) in Misner, Thorne and Wheeler [9] and study test particles in a relativistic scalar gravitational theory (see also ST). The field equation for the scalar gravitational field Φ is

$$\square\Phi = 4\pi e^{\Phi}\rho, \quad (2.1)$$

where the metric is the flat Minkowski metric

$$g_{\alpha\beta} = \eta_{\alpha\beta}^{\text{flat}}. \quad (2.2)$$

Note that the exponential term on the right hand side makes the field equation nonlinear. For a single particle of rest mass m , traveling along its worldline $z^\mu(t)$, the comoving density ρ can be written

$$\rho = m \frac{\delta^3[x^a - z^a(t)]}{\gamma\sqrt{-g}} = \frac{\rho_0}{\gamma}, \quad (2.3)$$

where $\gamma = \dot{z}^0$ is the Lorentz factor and ρ_0 is the density in the stationary frame. The particle follows a geodesic

$$\frac{Du^\mu}{d\tau} + [g^{\mu\nu} + u^\mu u^\nu]\Phi_{,\nu} = 0, \quad (2.4)$$

where D denotes covariant differentiation and $u^\mu = dz^\mu/d\tau$ is the 4-velocity.

Conservation of energy-momentum follows from

$$\nabla \cdot \mathbf{T} = 0, \quad (2.5)$$

where the stress-energy tensor $T^{\mu\nu}$ can be decomposed into a gravitational field part and a matter part:

$$T_{\mu\nu} = T_{\mu\nu}^{\text{field}} + T_{\mu\nu}^{\text{particle}}, \quad (2.6)$$

where

$$T_{\mu\nu}^{\text{field}} = \frac{1}{4\pi} [\Phi_{,\mu}\Phi_{,\nu} - \frac{1}{2}g_{\mu\nu}\Phi_{,\sigma}\Phi_{,\sigma}], \quad (2.7)$$

$$T_{\mu\nu}^{\text{particle}} = \rho e^{\Phi} u_\mu u_\nu. \quad (2.8)$$

Note that the field equation (2.1) can be rewritten

$$\square\Phi = -4\pi T^{\text{particle}}, \quad (2.9)$$

where $T^{\text{particle}} = g^{\mu\nu}T_{\mu\nu}^{\text{particle}}$.

Matter conservation is expressed by the condition

$$\nabla \cdot \vec{J} = 0, \quad (2.10)$$

where the components of the matter current density are $J^0 = \gamma\rho$ and $J^i = \gamma\rho v^i$. Here v^i is the usual three-velocity.

The above equations can be generalized to a swarm of particles by letting

$$m \rightarrow \sum_A m_A, \quad u^\mu \rightarrow u_A^\mu, \quad \text{etc.} \quad (2.11)$$

(see equation (2.16) and related paragraph in ST).

Integrating (2.10) over all space yields a conserved rest mass

$$M_0 = \int J^0 d^3x = \int \gamma\rho d^3x = \int \rho_0 d^3x = \text{const.} \quad (2.12)$$

Combining the integrals of Eq. (2.5) and Eq. (2.10) gives rise to a conserved total energy at any time t inside a sphere of arbitrary radius r centered at the origin:

$$E_{\text{tot}} = E_1 + E_2 + E_3. \quad (2.13)$$

Here E_1 is the energy of the gravitational field, including a dynamical component,

$$E_1 = \frac{1}{8\pi} \int_0^r r'^2 dr' \int (\Phi_{,t}^2 + (\nabla\Phi)^2) d\Omega, \quad (2.14)$$

E_2 is the particle's kinetic and gravitational binding energy,

$$E_2 = \int_0^r r'^2 dr' \int \rho_0 (e^{\Phi}\gamma - 1) d\Omega, \quad (2.15)$$

and E_3 is the total outgoing flux of particles and radiation across r , integrated over all time,

$$E_3 = -r^2 \int_0^t dt' \int d\Omega \left[\frac{1}{4\pi} \Phi_{,t}\Phi_{,r} - \rho_0 v_r (e^{\Phi}\gamma - 1) \right]. \quad (2.16)$$

Since the total energy is conserved, and since E_3 vanishes initially, E_{tot} at all times has to be equal to the sum of E_1 and E_2 at $t = 0$,

$$E_{\text{tot}}(0) = \int_0^r r'^2 dr' \int d\Omega \left[\frac{1}{8\pi} (\Phi_{,t}^2 + (\nabla\Phi)^2) + \rho_0 (e^{\Phi}\gamma - 1) \right]_{t=0}. \quad (2.17)$$

As shown in ST, the total conserved mass-energy $M = \int T^{00} d^3x$ is related to E_{tot} according to $M = M_0 + E_{\text{tot}}$.

The radiative energy flux in the wave zone is

$$T_{\text{field}}^{0r} = -\frac{1}{4\pi}\Phi_{,t}\Phi_{,r} \approx \frac{1}{4\pi}\Phi_{,t}^2, \quad (2.18)$$

and the total rate of energy emission

$$\frac{dE_{\text{field}}}{dt} = 4\pi r^2 T_{\text{field}}^{0r} \approx (r\Phi_{,t})^2. \quad (2.19)$$

Note that these expressions become exact as $r \rightarrow \infty$.

In the weak-field, slow-motion limit, the radiation field can also be expressed as a multipole expansion, which we will use to compare with our QE approximation. Since the theory involves a scalar field, the lowest-order contribution to the radiation arises from the monopole term. Using the usual Green's function for a wave equation, we follow ST and transform the wave Eq. (2.1) into the integral form

$$\Phi(t, r) = -\int d^3x' \frac{[e^\Phi \rho]_{\text{ret}}}{|\mathbf{x} - \mathbf{x}'|} \approx -\frac{1}{r} \int d^3x' \left[\frac{e^{2\Phi}}{\tilde{u}^0} \rho_0 \right]_{\text{ret}}, \quad (2.20)$$

where we have replaced $|\mathbf{x} - \mathbf{x}'|$ with $r = |\mathbf{x}|$ for large separations, and where “ret” means evaluate at retarded time $t' = t - |x - x'|$. For a spherically symmetric density distribution, the leading-order radiation field of Φ gives rise to the monopole formula

$$\Phi(t, r) = -\frac{4\pi}{r} \int dr' r'^2 \left[\rho_0 \left(\Phi - \frac{1}{2}v^2 \right) + \frac{1}{6}r'^2 \rho_{,tt} \right]_{t-r}. \quad (2.21)$$

This equation is the analogue of the “quadrupole formula” in general relativity (see also the discussion below eq. (3.8) in ST). Note again that scalar gravity admits gravitational radiation even in spherical symmetry, in contrast with GR.

B. Spherical matter shell

We now consider a thin, spherical shell of collisionless particles, all of the same rest mass m_A . At every point on the shell the particles move isotropically in the plane perpendicular to the radius. In an oscillating shell, each particle moves about the center in a bound orbit. In the Newtonian limit, each orbit is a closed ellipse.

In spherical symmetry, the geodesic equation (2.4) for a particle in the shell becomes

$$\frac{dR}{dt} = \frac{\tilde{u}_r}{\tilde{u}^0}, \quad (2.22)$$

$$\frac{d\tilde{u}_r}{dt} = \frac{\tilde{u}_\phi^2}{\tilde{u}^0 R^3} - e^{2\Phi} \frac{\Phi_{,r}}{\tilde{u}^0}, \quad (2.23)$$

$$\tilde{u}_\phi = \text{const}, \quad (2.24)$$

where

$$\tilde{u}^0 = \sqrt{e^{2\Phi} + \tilde{u}_r^2 + \tilde{u}_\phi^2/R^2}, \quad (2.25)$$

and where we have defined

$$\tilde{u}^a \equiv e^\Phi u^a. \quad (2.26)$$

Each particle orbits in a plane, conserving its orbital angular momentum \tilde{u}_ϕ . Note that it is sufficient to integrate the geodesic equations for one particle, which then represents the entire swarm. Note also that for a static gravitational field, the particle energy \tilde{u}^0 is constant.

The particle mass density is

$$\rho = \sum_A \frac{m_A}{\gamma} \delta(r - R) \delta(\theta - \theta_A) \delta(\phi - \phi_A) \frac{1}{r^2 \sin \theta}, \quad (2.27)$$

where (θ_A, ϕ_A) are distributed isotropically on a sphere. Inserting equation (2.27) into equation (2.12) yields

$$M_0 = \sum_A m_A, \quad (2.28)$$

so that smoothing out the particle distribution in the angular direction, we may rewrite the density as a purely radial function,

$$\rho = \frac{M_0}{4\pi R^2 \gamma} \delta(r - R), \quad (2.29)$$

where R is the radius of the shell.

In spherical symmetry, the field equation (2.1) can be written as

$$-\Phi_{,tt} + \frac{1}{r^2} (r^2 \Phi_{,r})_{,r} = 4\pi e^\Phi \rho. \quad (2.30)$$

Regularity at the origin requires the boundary condition

$$\Phi_{,r} = 0, \quad \text{at } r = 0, \quad (2.31)$$

and we impose an outgoing wave boundary condition at the outer boundary,

$$(r\Phi)_{,t} + (r\Phi)_{,r} = 0. \quad (2.32)$$

The delta function on the right hand side of (2.30) introduces a discontinuity in the first space derivative of Φ . Integrating the field equation across the shell yields the jump condition

$$\Phi_{,r}|_+ - \Phi_{,r}|_- = \frac{M_0}{R^2} \frac{e^{2\Phi}}{\tilde{u}^0}. \quad (2.33)$$

Note that Φ itself is continuous across the shell. In equation (2.23), the force term $\Phi_{,r}$ then has to be replaced by

$$\Phi_{,r} \rightarrow \frac{1}{2} (\Phi_{,r}|_+ + \Phi_{,r}|_-). \quad (2.34)$$

This expression can be found by properly averaging $\Phi_{,r}$ over an extended shell, and then taking the limit as the shell thickness goes to zero.

C. Static solutions

For static solutions, in which all particles are in circular orbits, the field equation (2.30) reduces to

$$\nabla^2 \Phi = \frac{1}{r^2} (r^2 \Phi_{,r})_{,r} = 4\pi e^\Phi \rho. \quad (2.35)$$

In vacuum, Φ is either constant or is proportional to r^{-1} . Given the boundary conditions (2.31) and (2.32), we therefore find solutions of the form

$$\begin{aligned} \Phi(r) &= -C, & r \leq R_S, \\ \Phi(r) &= -\frac{M_C}{r}, & r \geq R_S, \end{aligned} \quad (2.36)$$

where C and M_C are constants, and where R_S is the static equilibrium radius. Note that M_C determines the motion of distant particles and gives rise to Kepler's laws, so that it can be identified with a ‘‘Coulomb’’ mass, as discussed in ST. Unlike in GR, M_C does not agree with the total conserved mass-energy $M = M_0 + E_{\text{tot}}$ defined in (2.12) and (2.13).

Since Φ is continuous across the shell, we have

$$C = \frac{M_C}{R_S}, \quad (2.37)$$

and using the jump condition (2.33) yields

$$C = \frac{M_0}{R_S} \frac{e^{-2C}}{\tilde{u}^0}. \quad (2.38)$$

For a circular orbits we have $\tilde{u}^r = d\tilde{u}^r/dt = 0$, so that equation (2.23) yields

$$\tilde{u}_\phi^2 = \frac{e^{-2C}}{2} R_S^2 C, \quad (2.39)$$

and therefore

$$\tilde{u}^0 = e^{-C} (1 + C/2)^{1/2}. \quad (2.40)$$

Inserting this into (2.38) yields

$$C = \frac{M_C}{R_S} = \frac{M_0}{R_S} \frac{e^{-C}}{(1 + C/2)^{1/2}}. \quad (2.41)$$

Given M_0/R_S , equation (2.41) can be solved numerically for C or, equivalently, M_C/R_S . In the Newtonian limit, where M_0/R_S is small, we find

$$M_C = M_0 \left(1 - \frac{5}{4} \frac{M_0}{R_S} \right). \quad (2.42)$$

In the limit of large M_0/R_S , C and M_C/R_S scale with $\log(M_0/R_S)$, implying that unlike in GR, there is no maximum compaction M_C/R_S .

We can also combine equations (2.39) and (2.41) to obtain

$$\frac{e^{-2C}}{(2C - C^2)^{1/2}} = \frac{\tilde{u}_\phi}{M_0}. \quad (2.43)$$

Given M_0 and the angular momentum \tilde{u}_ϕ , this equation can be solved for C . The result can then be inserted into (2.39) to yield the radius R_S .

The oscillations which we consider in this paper are damped, and ultimately give rise to a static equilibrium state. During the damping process, both the rest mass M_0 and the angular momentum \tilde{u}_ϕ are conserved. Given any initial non-equilibrium configuration with M_0 and \tilde{u}_ϕ , we can therefore use (2.43) to determine the final equilibrium configuration to which the oscillating shell will ultimately settle down.

D. Newtonian limit

In the Newtonian limit, i.e. in the limit of weak fields and slow velocities, an analytic solution for a periodically oscillating shell can be derived (see Sect. VI of ST). Consider a static shell of rest mass M_0 and radius R_i , and reduce all velocities instantaneously by a factor ξ at $t = 0$. The individual particles comprising the shell then all move in elliptical orbits with the same period, eccentricity and semimajor axes satisfying

$$R = R_i x(t), \quad (2.44)$$

where $x(t)$ is given by the usual parametric equations for an elliptic orbit:

$$\begin{aligned} x &= a(1 + e \cos u), \\ t &= \frac{P}{2\pi} (u + e \sin u), \end{aligned} \quad (2.45)$$

Here the semimajor axis, eccentricity and period are, respectively

$$\begin{aligned} a &= \frac{1}{2 - \xi^2}, \\ e &= 1 - \xi^2, \end{aligned} \quad (2.46)$$

$$P = 2\pi \left(\frac{2R_i^3}{M_0(2 - \xi^2)^3} \right)^{1/2}.$$

The radial and tangential particle velocities are given by

$$\begin{aligned} v_r &= \frac{\dot{x}}{x} R, \\ v_\phi &= \xi \frac{r}{x^2} \left(\frac{M_0}{R_i^3} \right)^{1/2}. \end{aligned} \quad (2.47)$$

We have used this analytic solution extensively to test our code in the Newtonian limit.

Inserting the analytic solution into Eq. (2.21) and differentiating with respect to time yields the wave amplitude

$$\Lambda = r\lambda = -\frac{4}{3}\frac{M_0^2}{R_i}\left[\frac{\dot{x}}{x^2}\right]_{t-r}, \quad (2.48)$$

The total rate of energy emission can now be found from Eq. (2.19),

$$\frac{dE}{dt} = \frac{16}{9}\frac{M_0^4}{R_i^2}\left[\frac{\dot{x}^2}{x^4}\right]_{t-r}. \quad (2.49)$$

III. QUASI-EQUILIBRIUM SCHEME

In the QE approximation, we assume that the orbital decay time is much longer than the orbital period. On an orbital timescale, the effect of the gravitational radiation can then be neglected, and it is reasonable to assume that each orbit is determined by the ‘‘Coulomb’’ part of the gravitational field rather than the radiative part. This suggests that we can neglect the second time derivative in the field equation (2.1), so that the field then satisfies the elliptic equation

$$\nabla^2\Phi = 4\pi e^\Phi \rho_{\text{QE}}. \quad (3.1)$$

Similarly, QE approximations in GR typically lead to elliptic equations for the gravitational field components (see, e.g., [12,3,4]). This approximation greatly simplifies the problem, since the gravitational field no longer has any dynamical degrees of freedom.

Since no radiation is generated in the QE approximation, the system is strictly conservative and there is a conserved energy E_{QE} . This energy can be derived by multiplying equation (2.23) with $2\tilde{u}_r$, which yields

$$\frac{d\tilde{u}_r^2}{dt} = -\frac{d}{dt}\frac{\tilde{u}_\phi^2}{R^2} - 2e^{2\Phi_{\text{sh}}}\Phi_{,r}\frac{dR}{dt}. \quad (3.2)$$

Here $\Phi_{\text{sh}} = \Phi(R)$, and we have used conservation of angular momentum $\tilde{u}_\phi = \text{const.}$ From Eqs. (2.34) and (2.36) we also have

$$\Phi_{,r} = -\frac{\Phi_{\text{sh}}}{2R}. \quad (3.3)$$

Using (2.38), we can now rewrite eq. (3.2) as

$$\frac{d}{dt}\left(\tilde{u}_r^2 + \frac{\tilde{u}_\phi^2}{R^2}\right) = -\frac{\tilde{u}^0\Phi_{\text{sh}}^2}{M_0}\frac{dR}{dt}. \quad (3.4)$$

Expressing the left hand side in terms of \tilde{u}^0 (eq. (2.25)), we finally find

$$E_{\text{QE}} \equiv M_0\tilde{u}^0 + \frac{1}{2}R\Phi_{\text{sh}}^2 = \text{const.} \quad (3.5)$$

In order to relate E_{QE} to the conserved total energy E_{tot} (eq. (2.13)), we evaluate the latter in the QE approximation by inserting the solution (2.36) and by setting the radiative components of the field equations to zero: $\Phi_{,tt} = \Phi_{,t} = 0$. We then find

$$\begin{aligned} E_1 &= \frac{1}{2}\int_0^r (\nabla\Phi)^2 r'^2 dr', \\ &= -\frac{1}{2}\Phi_{\text{sh}}^2 R^2 \int_R^r \frac{dr'}{r'^2} = -\frac{1}{2}\Phi_{\text{sh}}^2 R^2 \left(\frac{1}{r} - \frac{1}{R}\right) \end{aligned} \quad (3.6)$$

and

$$E_2 = \int_0^r r'^2 dr' \int \rho_0(\tilde{u}^0 - 1)d\Omega = M_0(\tilde{u}^0 - 1). \quad (3.7)$$

The radiative contribution E_3 in (2.13) vanishes identically. We therefore have

$$E_{\text{tot}} = E_1 + E_2 = M_0(\tilde{u}^0 - 1) - \frac{1}{2}\Phi_{\text{sh}}^2 R^2 \left(\frac{1}{r} - \frac{1}{R}\right), \quad (3.8)$$

and find for $r \rightarrow \infty$

$$E_{\text{tot}} = E_{\text{QE}} - M_0 = \text{const.} \quad (3.9)$$

Note that this energy is conserved only when E_1 is evaluated with $r \rightarrow \infty$, so that it includes the entire potential energy of the longitudinal (or Coulomb-like) gravitational fields.

In the Newtonian limit,

$$\tilde{u}^0 = \gamma e^{\Phi_{\text{sh}}} = \frac{e^{\Phi_{\text{sh}}}}{\sqrt{1-v^2}} \approx 1 + \Phi_{\text{sh}} + \frac{1}{2}v^2. \quad (3.10)$$

Since to lowest order $\Phi_{\text{sh}} \approx -M_0/R$, we have

$$E_{\text{tot}} = \frac{1}{2}M_0v^2 - \frac{M_0^2}{2R} \quad (3.11)$$

in the Newtonian limit.

In the bottom panel of Fig. 1, we show E_{QE} as a function of apocenter radius R_{ap} for constant angular momentum $\tilde{u}_\phi = 1.17M_0^2$ (solid line). As we show in Appendix A, the turning point of this curve corresponds to an equilibrium configuration in which all particles move in circular orbits (see also Sec. II C). As the damped oscillations of the matter shell radiates energy, the shell ‘‘slides down’’ the energy curve in Fig. 1, until it settles down to static equilibrium at the curve’s minimum. We also include in the bottom panel of Fig. 1 the result of an exact evolution (dashed line), in which we started the oscillation with a static shell model at $R_i = 8M_0$, and then suddenly reduced all particle velocities by a factor of $\xi = 0.7$, so that the particle’s angular momentum is again $\tilde{u}_\phi = 1.17M_0^2$.

We now adopt a perturbative approach, in which we insert the predetermined QE matter density ρ_{QE} as a source to the fully dynamical field equations

$$\square\Phi(r, t) = 4\pi e^\Phi \rho_{\text{QE}}, \quad (3.12)$$

where ρ_{QE} is given by eqn. (2.29) using the QE solution for $R(t)$ (compare with the ‘‘hydro-without-hydro’’ approach as suggested in [7]). Integrating this equation then yields the periodic gravitational wave form and luminosity dE/dt for each QE configuration of a certain

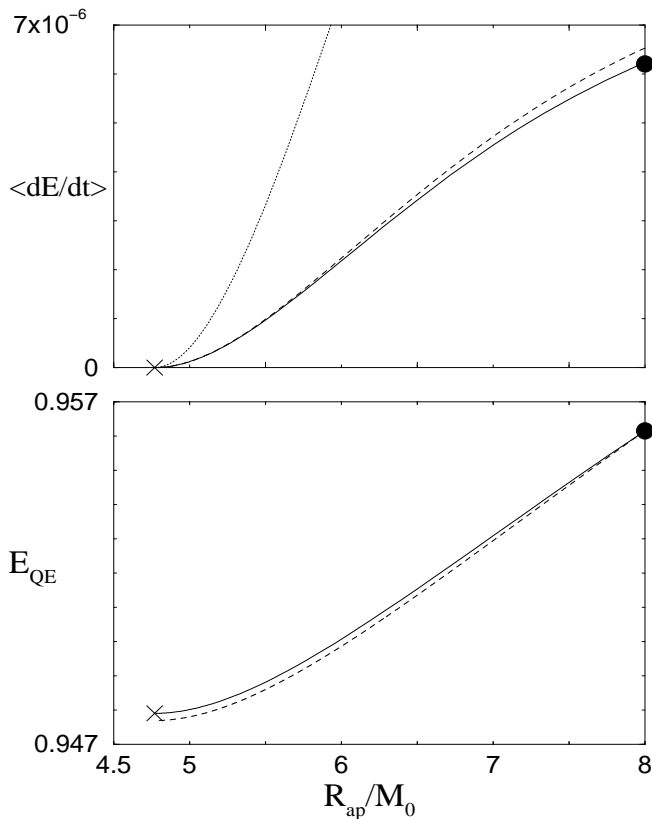


FIG. 1. The gravitational wave luminosity (upper panel) and the total energy (lower panel) as functions of apocenter radius (for a moderately strong field configuration, $R_i = 8M_0$, see Sec. IV B below). The dotted line denotes the result from the monopole formula (2.49), the dashed line shows the QE result, and the solid line shows the integration of the exact equations. In the lower panel, the dashed line is computed from eq. (3.5), and the solid line is computed from $E_{\text{QE}} \rightarrow E_1 + E_2 + M_0$ as in eq. (2.13) with $r \rightarrow \infty$.

apocenter radius. In practice, we determine dE/dt by averaging over one period P

$$\langle \frac{dE}{dt} \rangle = \frac{1}{P} \int_0^P \frac{dE}{dt} dt'. \quad (3.13)$$

We show $\langle dE/dt \rangle$ as computed from QE models in the top panel of Fig. 1 (solid line) and compare both with results from the integration of the exact equations (dashed line) and the monopole formulae (dotted line). From this plot it is already obvious that the QE “hydro-without-hydro” approach provides a much better approximation than the monopole formula. Combining $\langle dE/dt \rangle$ for several values of R_{ap} with the derivative of the QE energy $dE_{\text{QE}}/dR_{\text{ap}}$ then yields the damping rate

$$\frac{dR_{\text{ap}}}{dt} = \frac{\langle dE/dt \rangle}{dE_{\text{QE}}/dR_{\text{ap}}}. \quad (3.14)$$

(This is analogous to eq. (1) in [8] for binary neutron star inspiral.) Note that at the final equilibrium ra-

dius $R = R_S$, the numerator $\langle dE/dt \rangle$ vanishes more rapidly than the denominator $dE_{\text{QE}}/dR_{\text{ap}}$, so that dR_{ap}/dt smoothly approaches zero.

The complete wavetrain of the damped oscillations can be assembled by suitably parameterizing the wave signals for different values of R_{ap} (compare with eq. (2) in [8]). We provide details of this parameterization in Appendix B 2.

IV. NUMERICAL RESULTS

In this section, we compare results from the QE approach, the exact integration and the monopole formula for weak, moderately strong and ultra-strong fields. For each case, we prepare a static shell solution as in Sec. II C for a certain value of M_0/R_i , where R_i is the initial apocenter radius, and then reduce all velocities and hence angular momenta by a factor of $\xi = 0.7$. The particle orbits are then out of equilibrium and start a damped oscillation, until they lose sufficient energy by gravitational radiation to settle down into the final static equilibrium corresponding to the reduced value of the angular momentum.

Given the above scenario, the appropriate initial conditions for the gravitational field are

$$\Phi = \Phi_{\text{static}}, \quad \Phi_{,t} = 0, \quad (4.1)$$

where Φ_{static} is given by Eqs. (2.36) and (2.43). The particle initial data are

$$R = R_S, \quad \tilde{u}_r = 0, \quad \text{and} \quad \tilde{u}_\phi = \xi \tilde{u}_\phi^{\text{static}}, \quad (4.2)$$

where $\tilde{u}_\phi^{\text{static}}$ is given by (2.37) and (2.39). Thus the (non-equilibrium) shell begins at rest with all the particles at their apocenter positions.

For numerical reasons (involving the regridding algorithm as described in Appendix C), we found it convenient to impose outer boundary conditions at $5R_i$ (except for the strong field case, where we choose $50R_i$ for the outer boundary). We resolve the interior region of the shell with 50 gridpoints, and the exterior region with 200 gridpoints. The field integration scheme is adopted from ST and summarized in Appendix C.

A. Weak field configuration ($R_i = 1000M_0$)

We first study a weak field configuration with $R_i = 1000M_0$. After having reduced the angular momentum be a factor of $\xi = 0.7$, this configuration will ultimately settle down to a final radius of $R_f = R_S = 491.6M_0$. In Fig. 2 we compare the evolution of the shell’s radius as found from the integration of the exact equations (Sec. II B), the QE approach (Sec. III), and the analytic Newtonian result (Sec. II D). As expected, the agreement between the different approaches is excellent.

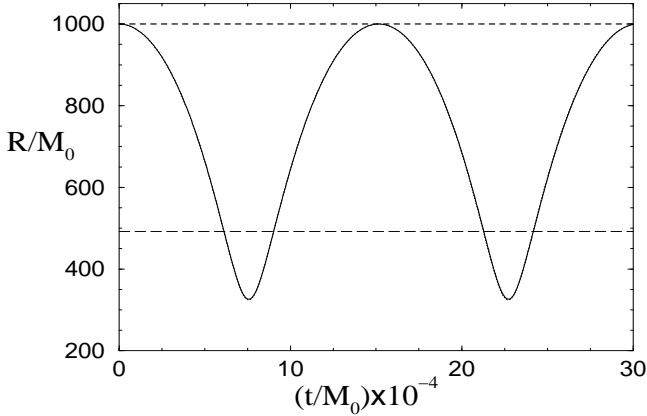


FIG. 2. Evolution of the radius as a function of time for a matter shell with the initial radius $R_i = 1000M_0$ and velocity cut-down factor $\xi = 0.7$. The solid line is the result from the integration of the exact equations. The dotted line, which completely coincides with the solid line, marks the analytic Newtonian result of Sec. IID. The short-dashed line is the envelope of apocenter radii oscillations according to the QE approach. The long-dashed line marks the final equilibrium radius of the shell.

In Fig. 3 we show that energy is conserved to very high accuracy in our code. Here, we evaluate the conserved integral (2.17) at radius $r = 1600M_0$. The plot also shows that the radiated energy E_3 (integrated flux) is very small compared with the other energy terms.

We show the QE parameters from which the QE waveform is constructed in Fig. 4. The gravitational radiation luminosity $\langle dE_{\text{QE}}/dt \rangle$ is computed by integrating eq. (3.12) for 13 different values of R_{ap} and interpolating between the results. Using (3.13) and (3.14), this can be combined with $dE_{\text{QE}}/dR_{\text{ap}}$ to yield the damping rate dR_{ap}/dt . The 4 parameters A , e_A , P , and e_P of the waveform (B12) and (B13) at different values of R_{ap} are determined by nonlinear data fitting (Appendix B). As expected, the values of e_A and e_P are very similar in the weak field case.

In Fig. 5 we compare the waveforms as obtained from the integration of the exact equations (solid line), the QE approach (dashed line) and the Newtonian analytic solution (dotted line) for the first 30 periods. The QE approach can reproduce the exact result very well. Note also that the QE scheme is very efficient: given an interpolation between the data for a small set of apocenter radii R_{ap} , the entire wavetrain, which in this case would take thousands of cycles and would, in an exact integration, be dominated by accumulation of numerical noise, can be constructed very easily.

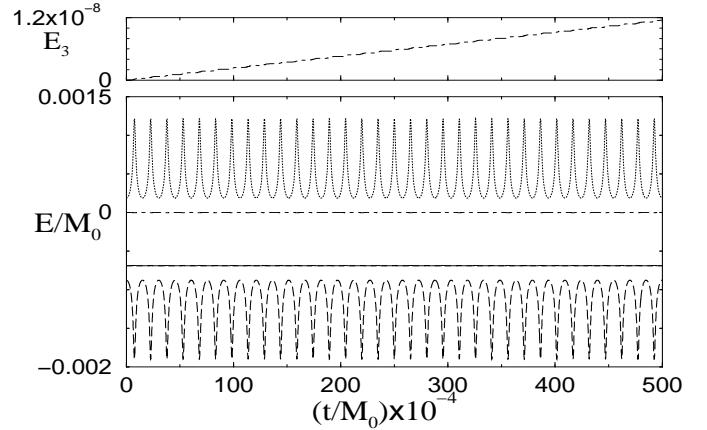


FIG. 3. Contributions to the total energy as a function of time for the weak field case $R_i = 1000M_0$. The solid line shows the total energy E_{tot} (see eq. (2.13)). The field energy E_1 is marked by the dotted line, the particle energy E_2 by the long-dashed line, and the integrated flux E_3 by the dot-dashed line (see also top panel). We also include the initial value of $E_{\text{tot}}(0)$, marked by a horizontal dashed line. The agreement between the solid and the dashed line demonstrates energy conservation and is a measure of the accuracy of our code.

B. Moderately strong field configuration ($R_i = 8M_0$)

We now turn to a configuration with a moderately strong field, $R_i = 8M_0$. In this case, the oscillation damps out much more quickly due to radiation reaction, and we can integrate the exact equations until equilibrium has essentially been reached. This occurs at $R = 4.77M_0$.

We show the evolution of the shell’s radius in Fig. 6. This plot includes the result from the integration of the exact equations (solid line) as well as the “envelope” $R_{\text{ap}}(t)$ as found in the QE approach. Fig. 7 shows the QE parameters which we have constructed for this configuration. We plot the energy contributions as a function of time in Fig. 8, and find that energy is conserved to about 0.4%. Computing the exact solution takes only a few CPU hours on, for example, an SGI O2 workstation.

Fig. 9 shows three waveforms of the oscillating shell. Here we compare the results of the QE and exact integrations with the result of the monopole formula when applied to the oscillating QE configurations. The QE waveform and the exact waveform agree very well up to late times ($t \sim 7000M_0$), at which point the oscillation amplitude has decreased by about a factor of 100. At this point the integration of the exact equations has accumulated substantial numerical noise, and may actually be less accurate than the QE approach. The waveform from the monopole approach disagrees with the exact one even at very early times, showing that the QE approach is much more reliable for moderately strong fields.

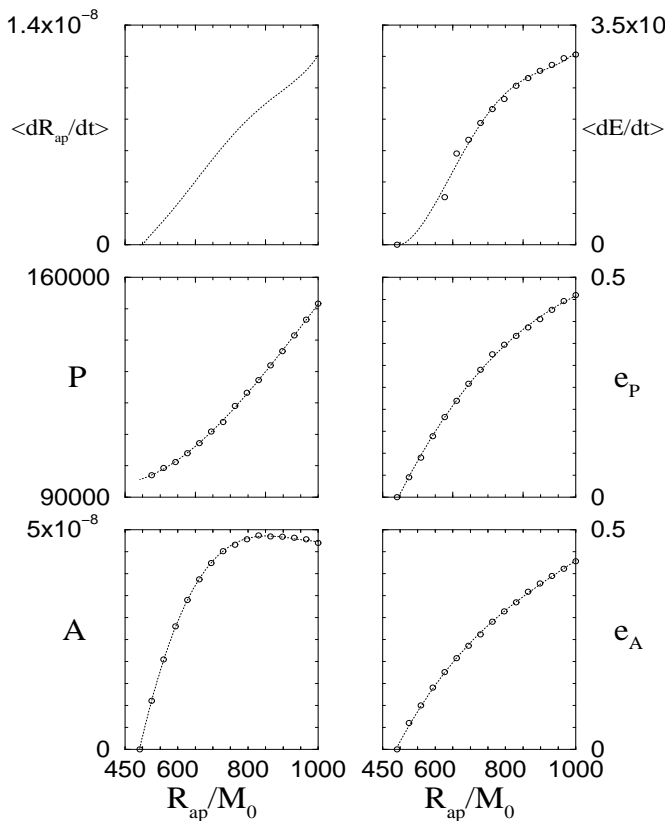


FIG. 4. Calculated QE data and their fitting curves as functions of apocenter radius for the $R_i = 1000M_0$ case. The circles are the calculated data points, and the dotted lines are the fitted curves.

C. Ultra-Strong field configuration ($R_i = 0.1M_0$)

For very strong fields, the oscillations are damped so strongly that our QE assumption no longer holds, and we therefore expect our QE approach to break down (see discussion below). Fig. 10 shows that the QE envelope $R_{\text{ap}}(t)$ no longer matches the exact result very well. We show the fitting parameters for this case in Fig. 11, and the energy contributions in Fig. 12 which still obey energy conservation quite well.

In Fig. 13 we compare the waveforms from the exact integration and the QE approach, and find the expected disagreement. Even here, however, the overall shape of the QE waveform is not far off. We do not include the monopole approximation, since its predictions do not even fit on the same scale.

We can illustrate the breakdown of the QE approach by the following simple argument. Figures 4, 7 and 11 show that dR_{ap}/dt decays like

$$\frac{dR_{\text{ap}}}{dt} \approx -\alpha(R_{\text{ap}} - R_f), \quad (4.3)$$

where the value of α depends on R_i/M_0 and can be read

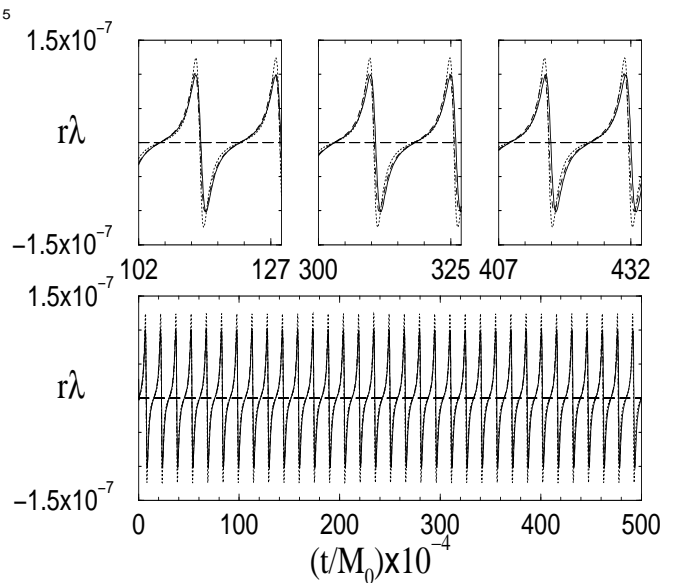


FIG. 5. Wave amplitude λ (multiplied by r) as a function of time at $r = 1600M_0$ for the weak field case ($R_i = 1000M_0$). The solid line shows the integration of the exact equations, the dashed line marks the QE result, and the dotted line is the monopole radiation obtained from the analytic Newtonian solution (see Sec. IID).

off of the above figures. As a result, R_{ap} decreases exponentially,

$$\frac{R_{\text{ap}} - R_f}{R_i - R_f} = e^{-\alpha t}. \quad (4.4)$$

The timescale $t_{\text{rad}} = \alpha^{-1}$ can now be compared to the orbital timescale t_{orb} . Inserting numbers for the three cases, we find

$$Q \equiv \frac{t_{\text{rad}}}{t_{\text{orb}}} \approx \begin{cases} 280000, & R_i = 1000M_0, \\ 15, & R_i = 8M_0, \\ 0.5, & R_i = 0.1M_0. \end{cases} \quad (4.5)$$

For the QE assumptions to hold we need $Q \gg 1$, which obviously holds only for $R_i = 1000M_0$ and $R_i = 8M_0$, but not for the ultra-strong field case $R_i = 0.1M_0$. It is therefore not surprising that the QE approach breaks down in this case.

We may also check the QE approximation, which neglects $\Phi_{,tt}$ in the field equation (2.1), for self-consistency. Assuming that $\Phi \sim 1/R$, we estimate its magnitude to be

$$\Phi_{,tt} \sim \frac{\ddot{R}}{R^2} - \frac{2\dot{R}^2}{R^3} \sim \frac{\dot{R}^2}{R^3} \quad (4.6)$$

and similarly

$$\nabla^2 \Phi \sim \frac{1}{R^3}. \quad (4.7)$$

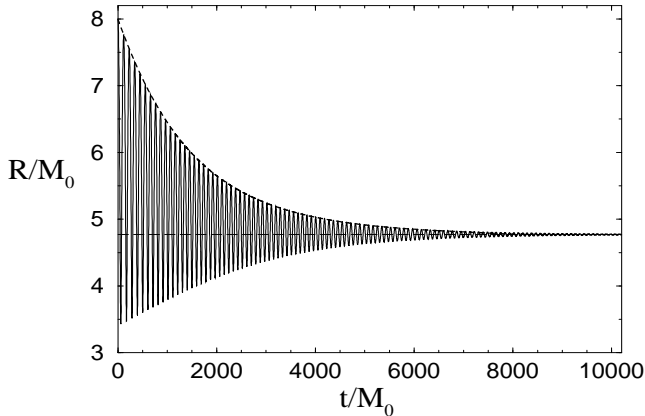


FIG. 6. Evolution of the shell radius as a function of time for a matter shell for the moderate field case ($R_i = 8M_0$). Labeling is the same as in Fig. 2, except that we do not include the Newtonian result.

The ratio of the two terms in equation (2.1) then becomes

$$\frac{\Phi_{,tt}}{\nabla^2\Phi} \sim \dot{R}^2 = v_r^2. \quad (4.8)$$

This suggests that $\Phi_{,tt}$ can be neglected, and hence that the QE approximation can be applied, only when $v_r^2 \ll 1$. In Figure 14 we show the maximum radial velocity for different values of R_i/M_0 , and also plot the ratio of $\Phi_{,tt}$ and $2\Phi_{,r}/R$ (which scales with $\nabla^2\Phi$, but is finite at the shell). This plot suggests that for $R_i/M_0 > 1$ we should expect errors less than a few percent, while for $R_i/M_0 = 1$, as in our ultra-strong field case, we should expect errors on the order of 10 %, which is consistent with our results.

V. CONCLUSION

In this paper, we illustrate our QE approach for calculating gravitational waveforms for a model problem in scalar gravitation. We demonstrate why it is a very viable technique to modeling binary inspiral in GR.

Compact binaries, consisting of neutron stars or black holes, emit gravitational wave and slowly spiral towards each other until they reach the ISCO. Outside of the ISCO, the inspiral is very slow: the gravitational radiation reaction timescale is much longer than the orbital period. It is therefore reasonable to assume the binaries to be in QE, and the inspiral to proceed along a sequence of QE configurations. In a recent paper, Duez, Baumgarte and Shapiro [8] demonstrated how the inspiral can be modeled by inserting QE binary models as matter sources in Einstein's field equations. Integrating Einstein's equations then yields the gravitational wave luminosity, from which the inspiral rate and hence the entire gravitational wavetrain can be constructed.

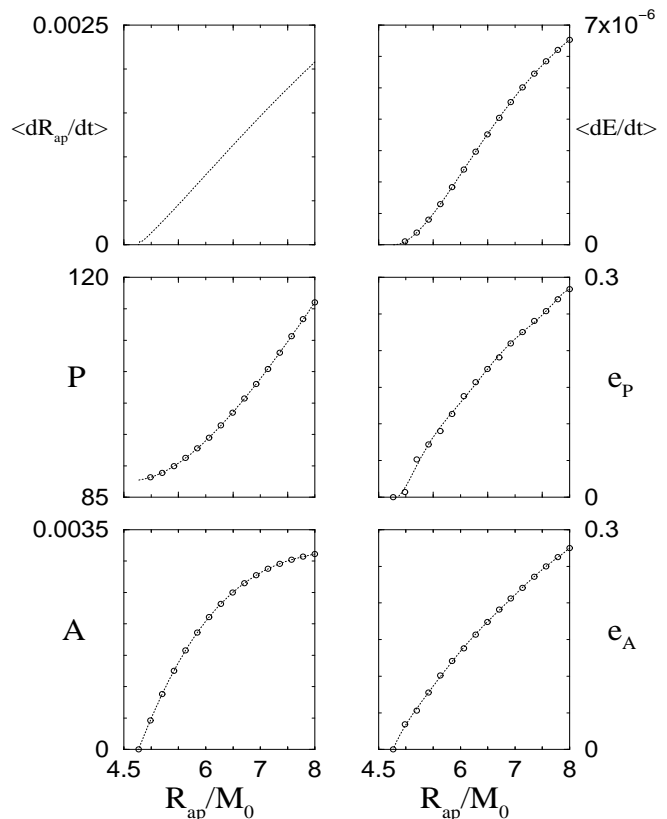


FIG. 7. Calculated data QE and their fitting curves as functions of apocenter radius for the moderately strong field case ($R_i = 8M_0$).

In this paper, we study a simple analogue in scalar gravitation. Scalar gravitation has the advantage that it is conceptually simpler, and that it admits gravitational radiation even in spherical symmetry, so that we can reproduce all qualitative characteristics of the QE approximation even in a 1 + 1 dimensional problem. We study the radiative damping of an oscillating, spherical matter shell. In analogy with the orbiting binary in GR, the oscillating shell emits gravitational radiation, and hence loses energy. While the binary separation decreases in the process, the oscillation amplitude decreases. Ultimately, the oscillation is completely damped out, and a static equilibrium configuration is reached.

The advantage of scalar gravitation is that it is possible to integrate the exact equations without any approximation. We compare these exact results with predictions from both our QE approach and the monopole approximation (which is the analogue of the quadrupole approximation in GR). We find that all three approaches agree very well for weak field solutions, but that the QE approach reproduces the exact solution much better for moderately strong fields. Only for ultra-strong fields does the QE approach break down.

We conclude that the QE approximation is a very promising approach to computing the adiabatic inspiral

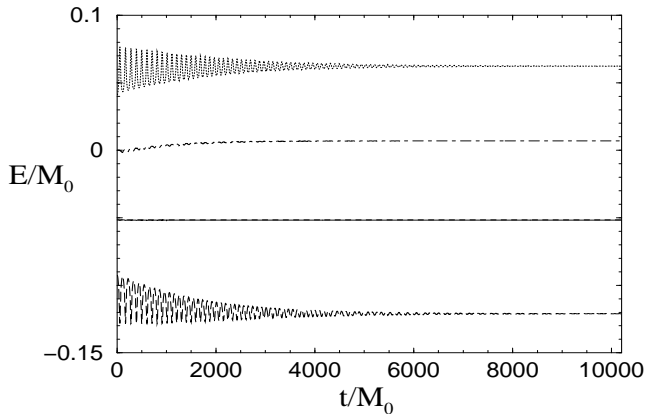


FIG. 8. Energy conservation as a function of time for the moderately strong field case ($R_i = 8M_0$). Labeling is the same as in Fig. 3.

of compact binaries.

ACKNOWLEDGMENTS

We thank M. Duez for useful discussions. This work was supported by NSF Grant PHY 99-02833 and NASA Grant NAG 5-7152 at the University of Illinois at Urbana-Champaign. TWB gratefully acknowledges support through a Fortner Fellowship. HJY acknowledges the support of the Academia Sinica, Taipei.

APPENDIX A: THE CORRESPONDENCE BETWEEN A TURNING POINT IN THE ENERGY CURVE AND STATIC EQUILIBRIUM

In this section we show that a turning point of the quasi-equilibrium energy E_{QE} versus apocenter radius R_{ap} ,

$$E_{QE} = M_0 \tilde{u}^0 + \frac{1}{2} R \Phi_{sh}^2, \quad (A1)$$

along a sequence of constant rest mass and angular momentum, coincides with an equilibrium configuration in which all particles are in circular orbits of radius R_C .

We evaluate E_{QE} at apocenter radius R_{ap} , where $\tilde{u}_r = 0$. Eq. (2.25) then yields

$$(\tilde{u}^0)^2 = e^{2\Phi_{sh}} + \frac{\tilde{u}_\phi^2}{R_{ap}^2}. \quad (A2)$$

For a sequence of constant rest mass and angular momentum we therefore find

$$\frac{d(M_0 \tilde{u}^0)}{dR_{ap}} = -R_{ap} \Phi_{sh} \frac{d\Phi_{sh}}{dR_{ap}} - \frac{\tilde{u}_\phi^2}{\tilde{u}^0 M_0 R_{ap}^3}, \quad (A3)$$

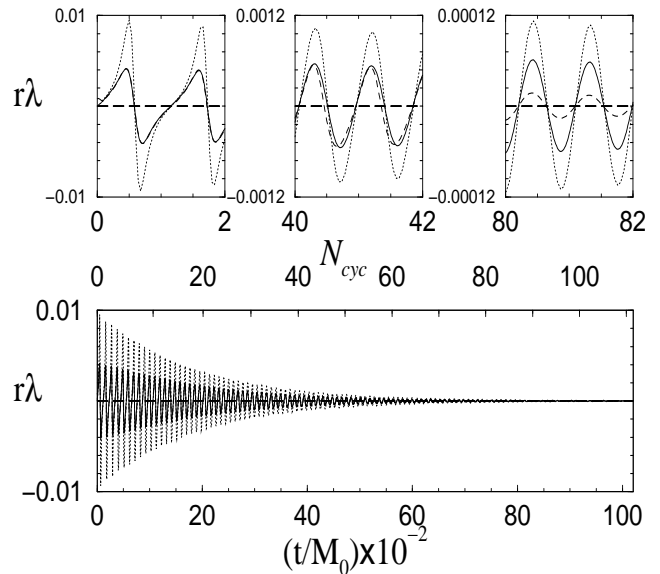


FIG. 9. Wave amplitude λ (multiplied by r) as a function of time as measured at $r = 10M_0$ for the moderate field case ($R_i = 8M_0$). Labeling is the same as in Fig. 5, except that the dotted line denotes the monopole formula applied to the oscillating QE shell.

where we have substituted eq. (2.38) in the form

$$\Phi_{sh} = -\frac{M_0 e^{2\Phi_{sh}}}{\tilde{u}^0 R_{ap}} \quad (A4)$$

to get eqn. (A3). The derivative of the second term in eq. (A1) is

$$\frac{d}{dR} \left(\frac{\Phi_{sh}^2 R_{ap}}{2} \right) = R_{ap} \Phi_{sh} \frac{d\Phi_{sh}}{dR_{ap}} + \frac{\Phi_{sh}^2}{2}. \quad (A5)$$

Combining eqs. (A3) and (A5) we now find

$$\frac{dE_{QE}}{dR_{ap}} = \frac{\Phi_{sh}^2}{2} - \frac{M_0 \tilde{u}_\phi^2}{\tilde{u}^0 R_{ap}^3}. \quad (A6)$$

At a turning point $dE_{QE}/dR_{ap} = 0$, which implies

$$\tilde{u}_\phi^2 = -\frac{e^{2\Phi_{sh}}}{2} R_S^2 \Phi_{sh}. \quad (A7)$$

Equation (A7) is equivalent to the result for static spherical shells, eq. (2.39). A turning point in the quasi-equilibrium energy therefore implies

$$R_{ap} = R_S, \quad (A8)$$

and hence coincides with a static equilibrium configuration.

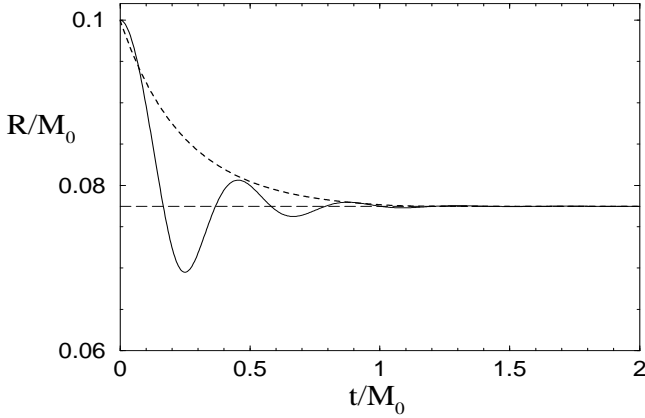


FIG. 10. Evolution of the radius as a function of time for the ultra-strong field case ($R_i = 0.1M_0$). Labeling is the same as in Fig. 2, except that we do not include the Newtonian result.

APPENDIX B: CONSTRUCTING THE CONTINUOUS QE WAVETRAIN

In this appendix we discuss the assembly of the QE solution and waveform. To do so, we construct QE solutions for a set of apocenter radii. We then evolve the gravitational fields dynamically in the presence of a QE matter source (see eq. (3.12)) to determine the gravitational wave form and luminosity for each apocenter radius. Guided by the analytical Newtonian expression for the shape of the waveform (see Sec. IID), we parameterize the waveform to be able to match the computed periodic data at discrete radii to a smooth function. In this Appendix we describe this parameterization together with a prescription for how the time evolution of these parameters can be determined. We illustrate our approach in Sec. B1, where we focus on the phase of the gravitational waves and its dependence on other parameters, and we construct the waveform template in Sec. B2.

1. Waveform phase versus time

Consider the simple example of an oscillator with constant period P and constant wave amplitude A . The waveform Λ can then be found from the phase θ , which in turn is given as a function of time:

$$\theta = \frac{2\pi}{P}t, \quad (\text{B1})$$

$$\Lambda = A \sin \theta. \quad (\text{B2})$$

In general, however, both A and P vary with time, in which case the phase, now denoted by ϑ can be computed from an integration

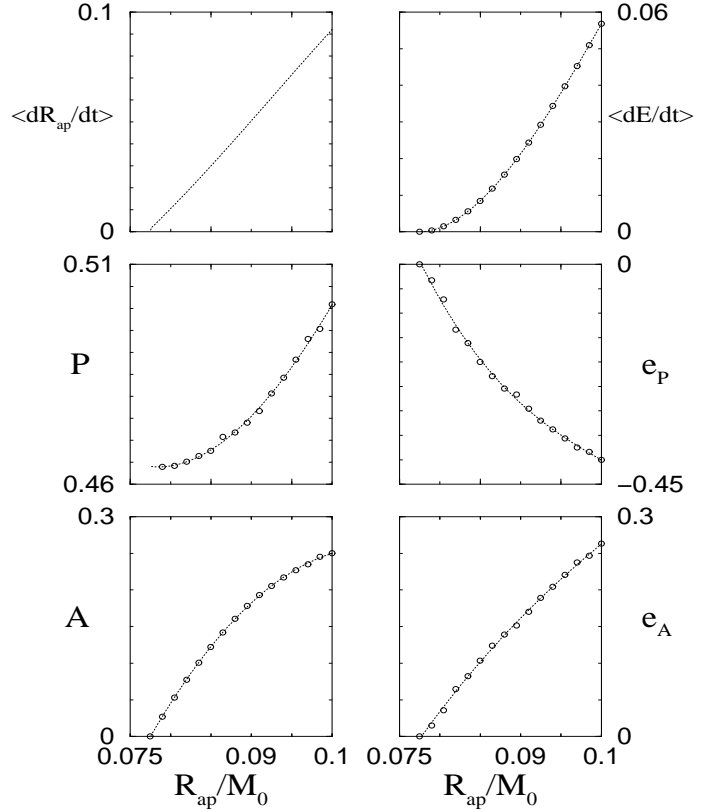


FIG. 11. Calculated QE data and their fitting curves as functions of apocenter radius for the ultra-strong field case ($R_i = 0.1M_0$). Labeling is the same as in Fig. 4

$$\vartheta = \int \frac{2\pi}{P(t)} dt, \quad (\text{B3})$$

$$\Lambda = A(t) \sin \vartheta.$$

In some cases, it is convenient to introduce a phase angle φ such that

$$\vartheta = \theta + \varphi, \quad (\text{B4})$$

where θ is given by eq. (B1). Taking a time derivative of this equation, we find

$$\frac{2\pi}{P} = \dot{\vartheta} = \dot{\theta} + \dot{\varphi} = \frac{2\pi}{P} - \frac{2\pi t}{P^2} \dot{P} + \dot{\varphi}, \quad (\text{B5})$$

where the first equality follows from (B3), the second from (B4), and the third from (B1). Comparing the left and right hand side, we find $\dot{\varphi} = 2\pi \dot{P}t/P^2$.

The relation between the phase θ and time t may be more complicated than eq. (B1), as for example in the Newtonian analytic solution for an oscillating shell, eq. (2.45). We therefore allow $\theta = \theta(t, p_i)$ to be a function of time t and a set of additional parameters $p_i(t)$, and generalize eqs. (B3) to

$$\vartheta = \int \partial_t \theta dt, \quad (\text{B6})$$

$$\Lambda = \Lambda(\vartheta, p_i).$$

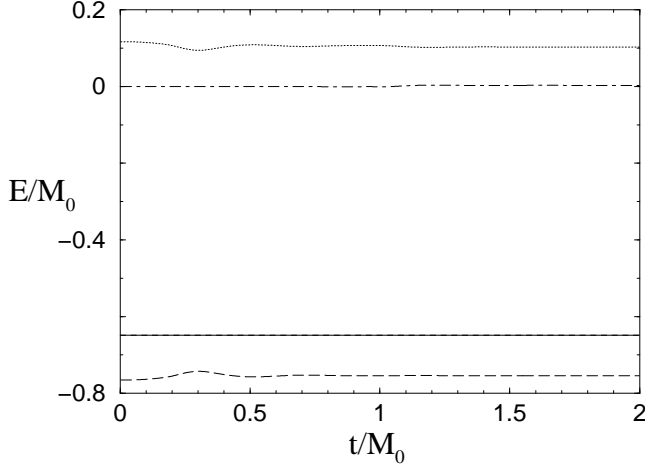


FIG. 12. Energy conservation as a function of time for the strong field case ($R_i = 0.1M_0$). Labeling is the same as in Fig. 3

We again introduce the phase angle φ

$$\vartheta = \theta + \varphi, \quad (\text{B7})$$

$$\partial_t \theta = \dot{\vartheta} = \dot{\theta} + \dot{\varphi} = \partial_t \theta + \Sigma \dot{p}_i \partial_{p_i} \theta + \dot{\varphi}, \quad (\text{B8})$$

and now find

$$\dot{\varphi} = -\Sigma \dot{p}_i \partial_{p_i} \theta. \quad (\text{B9})$$

This expression determines how the phase angle evolves when θ depends on several parameters. We will use this expression for the scalar wave model problem below.

2. QE parameterization and construction of the wave template

As described in Sec. III, we construct QE models for a set of apocenter radii and insert these as matter sources into the field equations as matter sources (eq. (3.12)). Dynamically evolving the gravitational fields will then yield the gravitational wave luminosity and the gravitational wave form. Given a suitable parameterization of the wave form, whose shape may be far from sinusoidal, we can find a set of parameters for each chosen value of the apocenter, and can then construct an interpolating function which yields all parameters as smooth functions of the apocenter (e.g. Figs. 4, 7 and 11). Combining the QE energy with the gravitational wave luminosity (eq. (3.14)) yields the damping rate and the entire evolution of the system. This enables us to express all parameters, and hence the waveform, as a continuous function of time.

A suitable wave from template can be constructed from the Newtonian analytical solution (see Sec. IID). Inserting eq. (2.45) into (2.48) yields

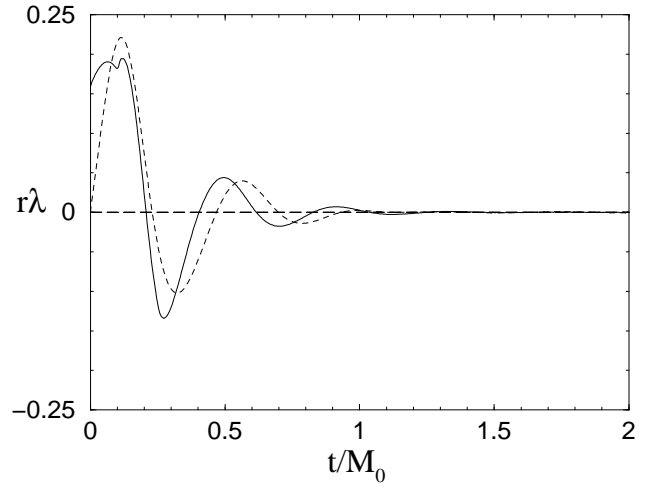


FIG. 13. Wave amplitude λ (multiplied by r) as a function of time as measured at $r = 0.8M_0$ for the ultra-strong field case ($R_i = 0.1M_0$). Labeling is the same as in Fig. 5, except that we do not include the Newtonian result. The small bump at early times is a numerical artifact and is due to slightly imprecise initial data.

$$t = \frac{P}{2\pi}(u + e \sin u), \quad (\text{B10})$$

$$\Lambda = \frac{8\pi}{3} \frac{M_0^2}{R_{\text{ap}}} \left[\frac{e \sin u}{aP(1 + e \cos u)^3} \right]_{t-r}. \quad (\text{B11})$$

We found that the fitting of the computed waveform to the above function in strong field configurations could be improved by allowing the eccentricity e in the two equations in eq. (2.45) to be different. This yields the template

$$t = \frac{P}{2\pi}(u + e_P \sin u), \quad (\text{B12})$$

$$\Lambda = \frac{A \sin u}{(1 + e_A \cos u)^3}. \quad (\text{B13})$$

We thus have four independent parameters P , e_P , A , e_A which we choose to characterize the waveform.

We construct QE configurations for 15 different apocenter radii R_{ap} between the initial radius R_i and the final circular radius R_f . At each value of R_{ap} we determine the four parameters P , e_P , A , e_A as well as the gravitational wave luminosity, $\Delta E/P$. We then construct interpolating functions, so that these parameters are now given as smooth functions of R_{ap} . Given the wave luminosity $\Delta E/P$ and the QE energy E_{QE} , the damping rate dR_{ap}/dt can be computed from eq. (3.14). The four parameters P , e_P , A , e_A , the wave luminosity $\Delta E/P$ and the damping rate dR_{ap}/dt are now all available as a function of apocenter radius R_{ap} . We show our results for weak, moderately strong and ultra-strong field cases in Figs. 4, 7 and 11.

As in Sec. B 1, we allow for a phase shift by introducing

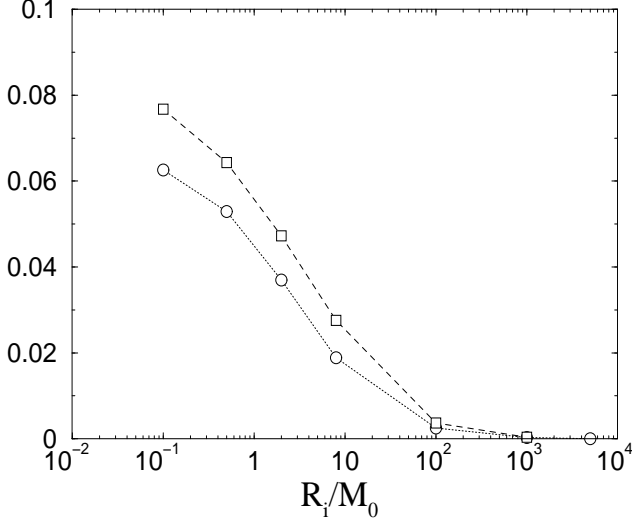


FIG. 14. The maximal value of the square of radial velocity v_r^2 (circles linked by the dotted line) and the dynamical part of the field equation $R\Phi_{,tt}/2\Phi_{,r}$ (squares linked by the dashed line) vs the initial radius. The size of these terms is a rough measure of the expected relative error in the QE approach.

$$\vartheta = u + \varphi, \quad (\text{B14})$$

where u satisfies eq. (B12), and where, according to eq. (B9), the phase angle φ evolves according to

$$\dot{\varphi} = -\dot{e}_P \partial_{e_P} u - \dot{P} \partial_P u = \frac{2\pi t \dot{P} + P^2 \dot{e}_P \sin u}{P^2(1 + e_P \cos u)}. \quad (\text{B15})$$

The wave form Λ is now given in terms of ϑ by

$$\Lambda = \frac{A \sin \vartheta}{(1 + e_A \cos \vartheta)^3}. \quad (\text{B16})$$

Here, the time derivative of the four parameters can be derived from the chain rule

$$\dot{p}_i \equiv \frac{dp_i}{dR_{\text{ap}}} \frac{dR_{\text{ap}}}{dt}. \quad (\text{B17})$$

The continuous waveform Λ can now be constructed by integrating the two equations

$$\dot{u} = \frac{2\pi - u\dot{P} - (e_P\dot{P} + P\dot{e}_P) \sin u}{P(1 + e_P \cos u)}, \quad (\text{B18})$$

$$\dot{\varphi} = \frac{2\pi t \dot{P} + P^2 \dot{e}_P \sin u}{P^2(1 + e_P \cos u)}. \quad (\text{B19})$$

$$(\text{B20})$$

The sum of the two yields ϑ , which, together with A and e_A , can then be inserted into eq. (B16) to give the entire gravitational wave train.

APPENDIX C: NUMERICAL ALGORITHM FOR INTEGRATING THE SCALAR WAVE EQUATION

In this Appendix, we outline our finite difference scheme, which is based on that of Ref. [10], and explain how the jump condition (2.33) is implemented in our code.

In spherical symmetry, the field Eq. (2.9) is

$$\Phi_{,tt} = \frac{1}{r^2} (r^2 \Phi_{,r})_{,r} + 4\pi T. \quad (\text{C1})$$

We rewrite this second order equation as two equations which are first order in time

$$\begin{aligned} \mathcal{T}[\Phi] &= \lambda, \\ \mathcal{T}[\lambda] &= \mathcal{R}[\Phi] + 4\pi T, \end{aligned} \quad (\text{C2})$$

where

$$\mathcal{T}[Y] \equiv Y_{,t}, \quad (\text{C3})$$

$$\mathcal{R}[Y] = 6[r^3 Y_{,r^2}]_{,r^3}. \quad (\text{C4})$$

Here Y denotes either Φ or λ . The Laplacian in the field equation is written in the form of (C4) to ensure regularity of the finite-difference operator near the origin. We implement a leapfrog scheme with a variable time step to solve these equations, and finite difference the operators $\mathcal{T}[Y]$ and $\mathcal{R}[Y]$ according to

$$\begin{aligned} \mathcal{T}_{i+1/2}^n[Y] &= \frac{\Delta t_{n-1}}{\Delta t_n + \Delta t_{n-1}} \frac{Y_{i+1/2}^{n+1} - Y_{i+1/2}^n}{\Delta t_n} \\ &+ \frac{\Delta t_n}{\Delta t_n + \Delta t_{n-1}} \frac{Y_{i+1/2}^n - Y_{i+1/2}^{n-1}}{\Delta t_{n-1}}, \end{aligned} \quad (\text{C5})$$

$$\begin{aligned} \mathcal{R}_{i+1/2}^n[Y] &= \frac{6}{r_{i+1}^3 - r_i^3} \left[r_{i+1}^3 \frac{Y_{i+3/2}^n - Y_{i+1/2}^n}{r_{i+3/2}^2 - r_{i+1/2}^2} \right. \\ &\quad \left. - r_i^3 \frac{Y_{i+1/2}^n - Y_{i-1/2}^n}{r_{i+1/2}^2 - r_{i-1/2}^2} \right], \end{aligned} \quad (\text{C6})$$

where $\Delta t_n = t_{n+1} - t_n$. These operators are second-order accurate in both space and time. At $r = r_{\text{max}}$ we impose an outgoing wave boundary condition

$$(rY)_{,t} + (rY)_{,r} = 0, \quad (\text{C7})$$

where Y is either Φ or λ . A second-order accurate finite difference form of this equation is

$$\begin{aligned} Y_{i_{\text{max}}+1/2}^{n+1} &= \frac{r_{i_{\text{max}}-1/2}}{r_{i_{\text{max}}+1/2}} Y_{i_{\text{max}}-1/2}^n + \frac{1-\zeta}{1+\zeta} \left[Y_{i_{\text{max}}+1/2}^n \right. \\ &\quad \left. - \frac{r_{i_{\text{max}}-1/2}}{r_{i_{\text{max}}+1/2}} Y_{i_{\text{max}}-1/2}^{n+1} \right], \end{aligned} \quad (\text{C8})$$

where

$$\zeta = \frac{\Delta t_n}{r_{i_{\max}+1/2} - r_{i_{\max}-1/2}}. \quad (\text{C9})$$

The jump condition (2.33) is easiest implemented by letting the grid move with the matter shell, so that $R_{\text{sh}} = r_{i_{\text{sh}}+1/2}$ at all times. The jump condition (2.33) can then be discretized to

$$\begin{aligned} r_{i_{\text{sh}}+1}^2 \frac{\Phi_{i_{\text{sh}}+3/2}^n - \Phi_{i_{\text{sh}}+1/2}^n}{r_{i_{\text{sh}}+3/2} - r_{i_{\text{sh}}+1/2}} - r_{i_{\text{sh}}}^2 \frac{\Phi_{i_{\text{sh}}+1/2}^n - \Phi_{i_{\text{sh}}-1/2}^n}{r_{i_{\text{sh}}+1/2} - r_{i_{\text{sh}}-1/2}} \\ = \frac{M_0}{\tilde{u}^0} e^{2\Phi_{i_{\text{sh}}+1/2}^n}. \end{aligned} \quad (\text{C10})$$

Eq. (C10) is used (by using a rootfinder) to derive the value of $\Phi_{i_{\text{sh}}+1/2}^{n+1}$ with the known values of $\Phi_{i_{\text{sh}}+3/2}^{n+1}$ and $\Phi_{i_{\text{sh}}-1/2}^{n+1}$ which are obtained from eqs. (C5) and (C6) in advance. After each time step, we interpolate the function values (at all three timelevels $n+1$, n and $n-1$) to a new grid, so that $r_{i_{\text{sh}}+1/2}$ at the new time level $n+1$ coincides with the new location of the matter shell R_{sh} . In our runs, we have chosen $i_{\text{sh}} = 50$. We use a uniform grid inside the shell, and a geometric progression, i.e., $r_{i+3/2} - r_{i+1/2} = \alpha(r_{i+1/2} - r_{i-1/2})$ where α is a fixed ratio, near unity, in the exterior.

Since all the particles making up the shell are identical, it is sufficient to evolve one particle. Moreover, since \tilde{u}_ϕ is a constant of the motion, only eqs. (2.22) and (2.23) need to be integrated to determine the particle's geodesic motion.

- [9] C. W. Misner, K. S. Thorne, and J. A. Wheeler, *Gravitation* (Freeman, San Francisco, 1973).
- [10] S. L. Shapiro and S. A. Teukolsky, Phys. Rev. D **47**, 1529 (1993) [ST].
- [11] S. L. Shapiro and S. A. Teukolsky, Phys. Rev. D **49**, 1886 (1994); M. A. Scheel, S. L. Shapiro and S. A. Teukolsky, Phys. Rev. D, **49**, 1894 (1994).
- [12] J. R. Wilson and G. J. Mathews, Phys. Rev. Lett. **75**, 4161 (1995).

-
- [1] K. S. Thorne, in *Black Holes and Relativistic Stars*, edited by R.M. Wald (U. of Chicago Press, Chicago, 1998), p. 62.
 - [2] T. Damour, P. Jaranowski and G. Schäfer, Phys. Rev. D **62**, 084011 (2000); L. Blanchet, T. Damour, B. R. Iyer, C. M. Will, and A. G. Wiseman, Phys. Rev. Lett **74** 3515 (1995).
 - [3] T. W. Baumgarte, G. B. Cook, M. A. Scheel, S. L. Shapiro and S. A. Teukolsky, Phys. Rev. Lett. **79**, 1182 (1997); Phys. Rev. D **57**, 7299 (1998).
 - [4] S. Bonazzola, E. Gourgoulhon, and J. A. Marck, Phys. Rev. Lett. **82**, 892 (1999); P. Marronetti, G. J. Mathews and J. R. Wilson, Phys. Rev. D **60**, 087301 (1999); K. Uryu and Y. Eriguchi, Phys. Rev. D **61**, 124023 (2000). K. Uryu, M. Shibata and Y. Eriguchi, submitted (also gr-qc/0007042).
 - [5] G. B. Cook, Phys. Rev. D **50**, 5025 (1994); T. W. Baumgarte, Phys. Rev. D **62**, 024018 (2000).
 - [6] S. L. Shapiro, paper presented at the Binary Neutron Star Grand Challenge Workshop, NCSA, Urbana, IL, January 1997.
 - [7] T. W. Baumgarte, S. A. Hughes and S. L. Shapiro, Phys. Rev. D **60**, 087501 (1999).
 - [8] M. D. Duez, T. W. Baumgarte and S. L. Shapiro, submitted (also gr-qc/0009064).